ORIGINAL ARTICLE

I-shaped ECC/UHPC composite beams reinforced with steel bars and BFRP sheets

Zhiqiang Dong [a, b], Jianghao Ji [a, b], Ziqing Liu [a, b], Chang Wu [a, b], Gang Wu [a, b, *], Hong Zhu [a, b], Pu Zhang [c]

[a]Key Laboratory of Concrete and Prestressed Concrete Structures of Ministry of Education, Southeast University, Nanjing 211189, China.
[b]National and Local Joint Engineering Research Center for Intelligent Construction and Maintenance, Nanjing 211189, China.
[c]Department of Civil Engineering, Zhengzhou University, Zhengzhou 450001, China.
* Corresponding author: Gang Wu. Email: g.wu@seu.edu.cn

Abstract: This paper proposes a new type of small-sized I-shaped engineered cementitious composite (ECC)/ ultra-high performance concrete (UHPC) composite beam which has the potential to be suitable for corrosive environments. The lower tensile part of the beam was made of ECC material (2/3 of the height), and the top compressive part was made of UHPC material (1/3 of the height). Inner embedded steel bars and surface-bonded basalt fiber reinforced polymer (BFRP) sheets were adopted as the reinforcing materials in combination. A total of nine I-shaped beams were designed and tested under four-point bending test. The influence of parameters such as the ratio of the embedded tensile steel bars, the top UHPC flange, and the surface bonded tensile BFRP sheet on the behavior of the beams was investigated. The results showed that the I-shaped ECC/UHPC composite beams have excellent comprehensive performance, and thanks to the ultra-high durability of the component materials, they have ultra-high durability that ordinary I-steel beams do not have and thus have broad application prospects in corrosive environments. The shear resistance capacity of the thin-walled ECC web needs to be further improved, and UHPC is recommended for the web in the follow-up study.

Keywords: I-shaped composite beam; ECC; UHPC; hybrid reinforcement; BFRP sheets

1 Introduction

Ordinary steel bars reinforced concrete (RC) structures and steel structures face severe durability problems in corrosive environments. In recent years, several popular new materials which have good corrosion resistance property have been developed and used, including the engineered cementitious composite (ECC), the ultra-high performance concrete (UHPC), and the fiber reinforced polymer (FRP), etc. The application of these new materials in civil engineering has been extensively studied. For example, in terms of the application of ECC, Fan et al. [1] adopted the ECC in the negative bending moment region of steel-concrete composite beams as a new solution to the cracking issue. Cai et al. [2-5] proposed a new type of ECC-encased concrete-filled steel tube (CFST) columns, and systematically investigated their performance under axial load, eccentric load, and seismic loading through model experiment and numerical simulation. Xiao et al [6-8] have conducted some studies on

ECC shell reinforced concrete structures and also discussed for 3d printed ECC. As to the application of UHPC which can have a compressive strength higher than 150 MPa, numerous studies have tried to place the UHPC in the compressive zone of composite members to utilize its high compressive performance. For example, composite beams with UHPC at the top compressive zone and NC at the bottom [9], profile steel-UHPC composite beams [10-12], and inverted-T steel girders with top UHPC slab [13-14]. To some extent, FRP can be regarded as a conventional material in civil engineering after more than 30 years research and application, especially in the field of structure retrofitting. Currently, the application of FRP is gradually expanding into new construction [15-19].

No material is perfect in all aspects of performance. For the new materials, they often need to be used in combination to maximize their advantages and minimize their shortages. For example, in recent years, scholars have carried out a lot of research on the combined application of FRP and ECC. Zhou et al. [20] pointed out in their research that even a thin ECC tension layer can significantly mitigate or eliminate the premature debonding of externally bonded FRP, thus maximizing the strengthening effectiveness of FRP sheets. Hu et al. [21] proposed a hybrid FRP-ECC strengthening system by replacing the corrosion-damaged concrete cover with ECC and attaching the FRP sheets to the soffit of the ECC layer. The FRP can not only be attached outside the ECC but can also be embedded in the ECC matrix to act as the load-carrying element. For example, Wu and Li [22] proposed a carbon-FRP (CFRP)-ECC hybrid system for strengthening concrete structures, the CFRP sheet was embedded in the ECC matrix, and the beams were tested under four-point bending. Test results indicated that the CFRP-ECC hybrid system is a good potential for the strengthening of concrete structures if the interface between ECC and concrete could be secured. Yang et al. [23] conducted an experimental study on the flexural performance of concrete beams strengthened with CFRP grids-reinforced ECC layer. Zheng et al. [24] proposed to use the FRP grid-reinforced ECC matrix composite to flexural strengthen the corrosion-damaged RC beams. Zheng et al. [25] and Guo et al. [26] investigated the shear strengthening effect of the FRP grid/ECC hybrid system on the RC beam.

In terms of new structures reinforced with FRP and ECC, Wang et al. [27] conducted an experimental study on the flexural performance of basalt-FRP (BFRP) bars reinforced seawater sea-sand concrete beams with textile reinforced ECC as the tensile protective layer. Ge et al. [28-29] conducted a series of studies on the flexural properties of FRP reinforced ECC-concrete composite beams (ECC was located at the lower part of the beam), and the reinforcement types included FRP bars, hybrid FRP/steel bars, and externally bonded carbon fiber sheets. In addition, Ge et al. [30] also conducted an experimental study on the flexural properties of FRP bars-reinforced ECC beams. Yuan et al. [31] investigated the seismic behavior of the hybrid FRP/steel bars reinforced concrete columns with normal concrete replaced by ECCs in the plastic hinge zone. Test results indicated that the replaced ECC efficiently eliminated the local buckling of the FRP bars and significantly improved the seismic performance of such hybrid reinforced columns.

In recent years, many studies have also been carried out on the combined application of FRP and UHPC. In the field of structural strengthening, for example, flexural strengthening of the positive moment sections of RC slabs with FRP, UHPC, and shear connector [32], flexural strengthening of RC beams with a hybrid system comprising of UHPC layer combined with near-surface-mounted (NSM) carbon-FRP (CFRP) strips in the beam bottom [33], and shear strengthening of corroded RC beams using UHPC combined with CFRP meshes [34]. In terms of new structures, researchers have proposed numerous forms of FRP-UHPC composite members. For example, UHPC beams reinforced with FRP bars [35-38], one-way BFRP bar-reinforced UHPC slabs [39], FRP fabrics reinforced UHPC panels [40], UHPC composite plates reinforced with FRP grids [41], lightweight UHPC-FRP composite decks [42], FRP bars reinforced seawater sea-sand concrete beams with a prefabricated UHPC shell [43], seawater sea-sand coral concrete-UHPC composite beams reinforced with BFRP bars [44], and so on.

In addition, researchers have also carried out many studies on the combination of FRP profiles and UHPC to form new members. For example, El-Hacha et al. [45-48] proposed a new type of pultruded box GFRP beams strengthened with a layer of UHPC on top and either a sheet of CFRP or steel-FRP on the bottom of the beam. The static and fatigue behavior under flexural loading, and the

shear behavior of the hybrid beams were systematically tested. Zou et. al. [49-50] and Zhang et. al. [51-52] conducted a series of studies on the combined use of the I-shaped pultruded FRP profile and an overlying UHPC slab for the application in bridges. In terms of vertical load-bearing members, numerous studies have been conducted on the UHPC columns confined by FRP sheet/tube [53-61]. Recently, two types of FRP-UHPC tubular permanent formwork were developed by Zeng et. al. [62] [63], one was internally reinforced with an FRP grid, and the other was internally reinforced with novel FRP micro-bars.
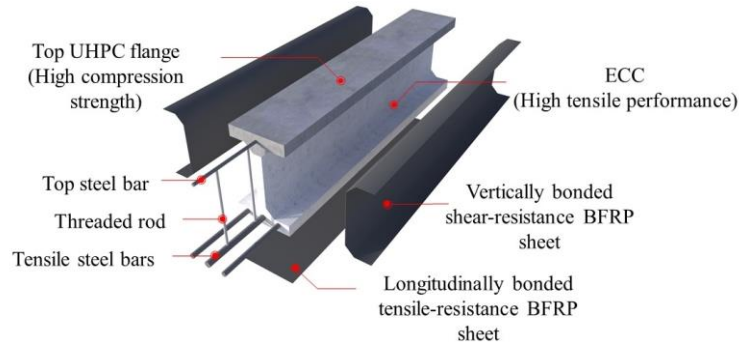
Fig. 1. The composition of the new type of I-shaped ECC/UHPC composite beam

Based on the above literature review, it can be seen that, from the perspective of complementary advantages, the combination of FRP, ECC, and UHPC to form a new lightweight, high-strength, and high-durability composite structure has broad application prospects. In this paper, a new type of small-sized I-shaped composite beam was innovatively proposed by the combined use of ECC, UHPC, and FRP. The composition of the hybrid beam is shown in **Fig. 1**. Since the ECC has excellent tensile performance with multiple and tight cracking nature, it was placed in the lower tensile part to improve the durability, the UHPC has superb compressive performance, and it was cast in the compression zone to improve the bearing capacity. As to the reinforcements, the BFRP sheet was longitudinally bonded at the bottom of the beam to improve the bearing capacity and durability, and vertically bonded BFRP sheets in the web were used to improve the shear resistance. In addition, for part of beams, threaded rods were embedded in the web to further improve the shear resistance. The properties of the proposed hybrid I-shaped beams were experimentally studied by four-point bending tests. It is well known that, in harsh service environments such as seaport terminals, chemical plants, coastal platforms, offshore platforms, and hydrophilic platforms, ordinary profile steel members are easily corroded, and long-term maintenance costs are high. The proposed novel high-durability small-sized I-shaped beams are expected to reasonably replace ordinary I-steel beams in the above-mentioned corrosive environments and expand the application scenario of new materials such as ECC, UHPC, and FRP in infrastructure.

Table 1. Mechanical properties of ECC and UHPC provided by the manufacturers

Product Model	Flexural strength (MPa)	Tensile strength (MPa)	Ultimate tensile strain (%)	Compressive strength (MPa)
ECC	12.0	3.0	2-4	30
UHPC	24.8	9.75	-	161

2 Materials

2.1 ECC and UHPC

The adopted high ductility engineered cementitious composite (ECC) was provided by the Henan Zhengda Building Materials Co., Ltd. The adopted fibers were PVA fibers with a length of 12 mm. The detailed mix ratio of the ECC was premixed compound: water: fiber =1: 0.25: 0.0034. The raw materials for producing the ultra-high performance concrete (UHPC) were provided by the Jiangsu Sobute New Materials Co., Ltd. The detailed mix ratio of the UHPC is premix compound (product name: SBT-UDC(II)): steel fiber: admixture (product name: PCA-I): tap water = 1000 g: 80 g: 12 g:

96 g. The adopted steel fibers have a length of 12 mm and a diameter of 0.13 mm. The cast I-shaped beams were immersed in room temperature tap water for 4 days and were then naturally cured in an ambient environment in the laboratory until testing. The mechanical properties provided by the manufacturer are shown in **Table 1**.

2.2 Reinforcement materials

The steel reinforcement cage embedded in the I-shaped beam consists of tensile steel bars in the bottom flange (8.0 mm and 10.0 mm), 5.0 mm threaded rods in the web, and a 5.0 mm plain steel bar at the top flange. The threaded rods are welded with the top plain steel bar and the bottom tension steel bar at an interval of 50 mm to form a reinforcement mesh. As mentioned in the introduction section, basalt-FRP (BFRP) sheets were vertically bonded on the web of the I-shaped beam to further improve the shear resistance of the thin-walled ECC web, and longitudinal BFRP sheets were bonded on the bottom flange to further improve the bending performance. The adopted unidirectional basalt fiber fabrics were provided by the Jiangsu Green Materials Valley New Material T&D Co., Ltd. The resin matrix used was provided by the Shanghai Sanyu Resin Co., LTD. The mechanical properties of the reinforcement materials used in this paper are shown in **Table 2**.

Table 2. Mechanical performance indices of the adopted reinforcement materials

Materials	Diameter (d) / Thickness (t)	Yielding strength (f_y)	Ultimate strength (f_u)	Elastic modulus (E_s, E_f)
Steel bars	8.0 mm and 10.0 mm	400 MPa	570 MPa	206 GPa
Threaded rods	5.0 mm	526 MPa	729 MPa	190 GPa
BFRP	0.35 mm (one layer)	-	668 MPa	32.6 GPa
BFRP	0.55 mm (two layers)	-	895 MPa	39.0 GPa

Notes: "-" means not available.

(a) E-0-0-0-0   (b) EU-0-0-0-0   (c) EU-Ø10-0-0-0   (d) EU-Ø10-0-FV-1FL   (e) EU-Ø10-0-FV-2FL

(f) E-Ø8/10-Ø5-FV-0   (g) EU-Ø8/10-Ø5-FV-0   (h) EU-Ø8/10-Ø5-FV-1FL   (i) EU-Ø8/10-Ø5-FV-2FL
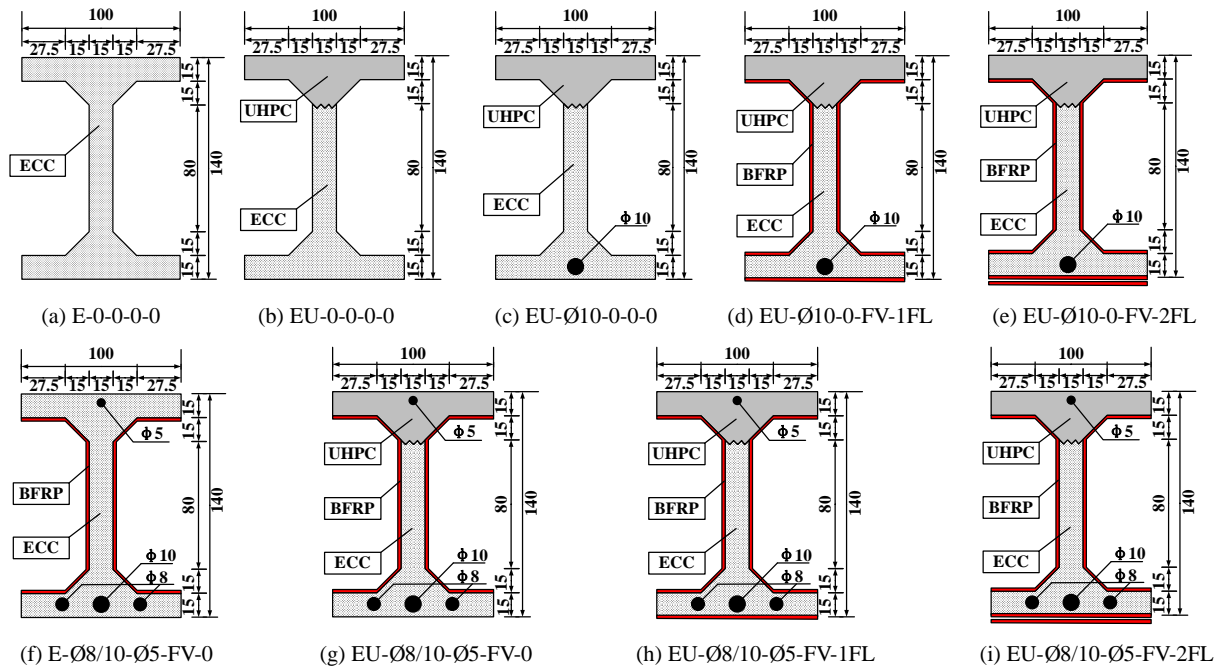
Fig. 2. Schematic diagram of the specimen cross-sectional size and reinforcement details (unit: mm)

3 Experimental program

3.1 Specimen sizes and test program

A total of nine small-sized I-shaped beams were prepared. The cross-sectional sizes and reinforcement details of the beams are shown in **Fig. 2**. The width is 100 mm, the height is 140 mm, and the thickness of the web and flanges are all 15 mm. Two kinds of reinforcement ratios are adopted

in the lower flange, one has a 10 mm steel bar, and the other has two 8.0 mm and one 10.0 mm steel bars. For the beams with a higher reinforcement ratio, to improve the shear resistance of the thin-walled web, threaded rods with a diameter of 5.0 mm were placed at an interval of 50 mm in the web. Part of the specimens are bonded with BFRP sheets on both sides of the thin-walled web to further enhance the shear-resistant capacity of the web, and some beams are attached with one or two layers of BFRP sheet on the bottom of the flange to improve the flexural bearing capacity.

The detailed test program is shown in **Table 3**. The specimens are numbered in the form of "A-B-C-D-E", where the first letter "A" represents the type of cement-based material used, among which, the "E" represents ECC, the "EU" represents composited ECC and UHPC; the second letter "B" represents the containing or not of the tension steel rebars in the bottom flange, among which, the "0" represents no steel bars, the "Ø10" represents one 10 mm steel bar, and the "Ø8/10" represents two 8 mm steel bars and one 10 mm steel bar; the third letter "C" represents whether threaded rods are embedded in the web, among which, the "0" means not configured, the "Ø5" means configured; the fourth letter "D" represents whether bonded with the vertical BFRP sheet or not, among which, the "0" means no vertical BFRP sheet, the "FV" means that there are vertical BFRP sheets; the fifth letter "E" represents whether longitudinal tensile BFRP is bonded on the bottom flange, among which, the "0" means no longitudinal BFRP sheet, the "1FL" means one layer of longitudinal tensile BFRP sheet attached, "2FL" means two layers of longitudinal tensile BFRP sheets attached.

Table 3. Test program

Specimens No.	Cement-based materials	Reinforcements inside bottom flange (mm)	Shear reinforcement inside web (mm)	Shear BFRP	Tensile BFRP
E-0-0-0-0	ECC	-	-	-	-
EU-0-0-0-0	ECC and UHPC	-	-	-	-
EU-Ø10-0-0-0	ECC and UHPC	1×10.0	-	-	-
EU-Ø10-0-FV-1FL	ECC and UHPC	1×10.0	-	1-layer	1-layer
EU-Ø10-0-FV-2FL	ECC and UHPC	1×10.0	-	1-layer	2-layer
E-Ø8/10-Ø5-FV-0	ECC	2×8.0+1×10.0	5.0@50.0	1-layer	-
EU-Ø8/10-Ø5-FV-0	ECC and UHPC	2×8.0+1×10.0	5.0@50.0	1-layer	-
EU-Ø8/10-Ø5-FV-1FL	ECC and UHPC	2×8.0+1×10.0	5.0@50.0	1-layer	1-layer
EU-Ø8/10-Ø5-FV-2FL	ECC and UHPC	2×8.0+1×10.0	5.0@50.0	1-layer	2-layer

Notes: To facilitate the crack testing by the 3D-DIC method, vertical BFRP sheets were not bonded to the pure bending section, "-" means not available.

3.2 Specimens preparation process

The preparation process of the I-shaped ECC/UHPC composite beams is shown in **Fig. 3**. As shown in **Fig. 3**a, First, the internal steel reinforcement cage was manufactured, in which the web was threaded rods with a diameter of 5.0 mm and a spacing of 50 mm, the top was an HPB 235 plain steel bar with a nominal diameter of 5.0 mm, and the bottom steel bars were HRB400 ribbed steel bars with a nominal diameter of 10.0 mm and 8.0 mm (some specimens contain only one 10.0 mm steel bar). **Fig. 3**b shows the casting process of the composite beams, the wooden formwork was placed on the vibrating table to ensure the compactness of the ECC and UHPC. For beams containing two types of cement materials, the ECC was cast and compacted firstly, and then the UHPC was poured and compacted straight after. As shown in **Fig. 3**c, all beams were cast on September 1, 2021, and were cured in the laboratory ambient environment for five days before demolding, and then immersed in room temperature tap water for 4 days. Finally, the specimens were polished to paste the BFRP sheets (**Fig. 3**d). The bonding process of BFRP sheets is shown in **Fig. 3**e. First, the BFRP sheet on webs was bonded, and then the bottom tensile BFRP sheet was bonded. After finalizing the bonding of

BFRP sheets, all beams were placed in the laboratory ambient environment for further curing until testing.

(a) Steel reinforcement cage   (b) Casting ECC and UHPC

(c) Specimens after cast   (d) Specimens after demolded   (e) Attaching the BFRP sheets
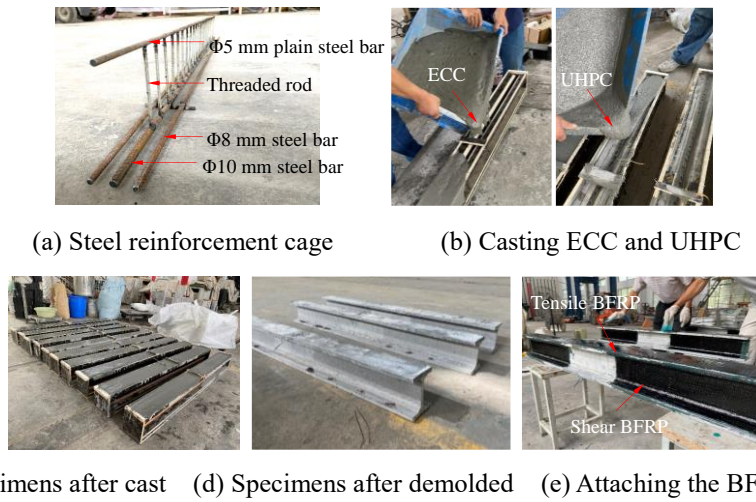
Fig. 3.   Specimen preparation process

3.3 Test set-up and instrumentations

The test set-up and the layout of instrumentations are shown in **Fig. 4**. The I-shaped composite beams were loaded with four-point bending over a simply supported clear span of 1200 mm and a 400 mm shear span, resulting in a nominal shear-span ratio of 2.86. The load was continuously applied with a hand-operated hydraulic jack at a rate of approximately 2.5 kN/min. Three linear variable differential transducers (LVDTs) were placed to measure the deflections at the mid-span and the two loading points, and two LVDTs were placed at the two supports to offset its settlement. Strain gauges (SGs) with a length of 100 mm were attached to the side of the I-shaped beam to monitor the tensile or compressive strains at the mid-span. All measurements, including load, displacement, and strain, were recorded by a TDS530 data acquisition system. Meanwhile, the non-contact 3D-digital image correlation (DIC) testing technology was used to real-time monitor the full-field strain and visually display the development of cracks in the beams.

(a) Layout of instrumentations (unit: mm)   (b) 3D schematic diagram of the test setup
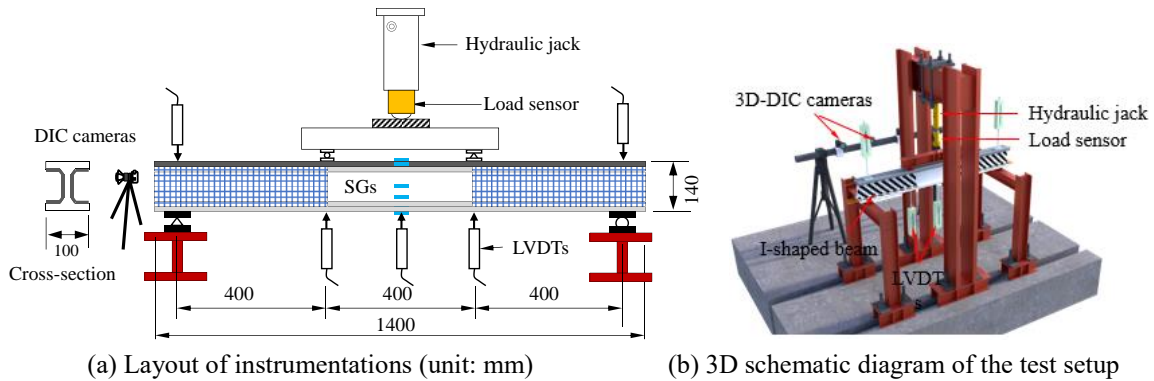
Fig. 4.   Test set-up and instrumentations

4 Test results

4.1 Failure modes

Fig. 5 shows the failure modes of all beams tested in this paper. **Fig. 5**a shows the failure mode of the pure ECC beam without reinforcements. When it fails, a main crack appears in the mid-span, and dense micro-cracks appear on both sides of the main crack. The ECC in the compression zone does not crush at the ultimate stage. **Fig. 5**b shows the failure mode of the un-reinforced composite beam with the top ECC flange replaced by UHPC. It can be seen that the un-reinforced composite beam failed due to the tensile crack of ECC at the loading point, and the top compression UHPC did

not crush. Thanks to the high tensile capacity of the ECC, although there is no reinforcement inside, both the E-0-0-0-0 beam and EU-0-0-0-0 beam do not show a brittle failure after cracked. There are many fine microcracks next to the main crack, and PVA fibers can be seen across the cracks at the bottom of the beam.

As shown in **Fig. 5**c, compared to the EU-0-0-0-0 beam, an additional 10 mm HRB400 steel bar is embedded in the bottom ECC flange of the EU-Φ10-0-0-0 beam. It can be seen that shear failure occurred in the EU-Φ10-0-0-0 beam, and dense and fine inclined cracks appeared in the bending-shear area. The inclined cracks initiated from the support to 150 mm away from the loading point. As shown in **Fig. 5**d, a layer of BFRP sheet is attached to the bottom and web of the I-shaped beam as additional reinforcements. It can be seen that the attachment of one layer of the BFRP sheet to the web cannot effectively avoid the shear failure. When the beam is damaged, the bottom flange and web in the flexural shear zone are dislocated along the beam length direction. The analysis shows that this might be caused by the tension force of the BFRP sheet that is transmitted to the beam end. As shown in **Fig. 5**e, for the EU-Φ10-0-FV-2FL beam which has two layers of BFRP sheets, the top UHPC flange in the bending shear area is separated from the ECC web in the failure stage, and the top UHPC flange in the bending shear area is fractured upward at a distance of 250 mm from the loading point.
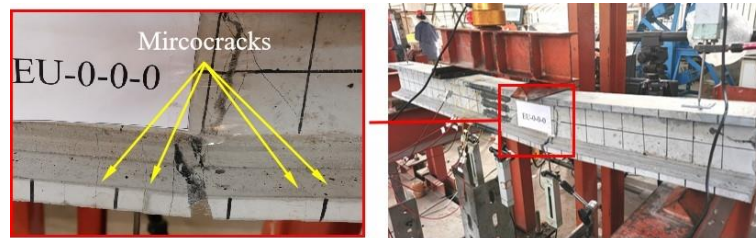
(a) E-0-0-0-0

(b) EU-0-0-0-0

(c) EU-Ø10-0-0-0

(d) EU-Ø10-0-FV-1FL

(e) EU-Ø10-0-FV-2FL

(f) E-Ø8/10-Ø5-FV-0

(g) EU-Ø8/10-Ø5-FV-0

(h) EU-Ø8/10-Ø5-FV-1FL

(i) EU-Ø8/10-Ø5-FV-2FL
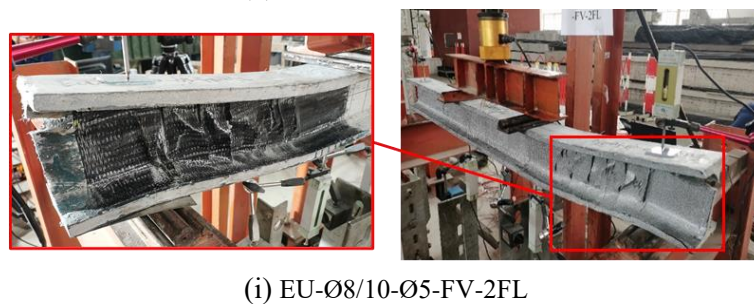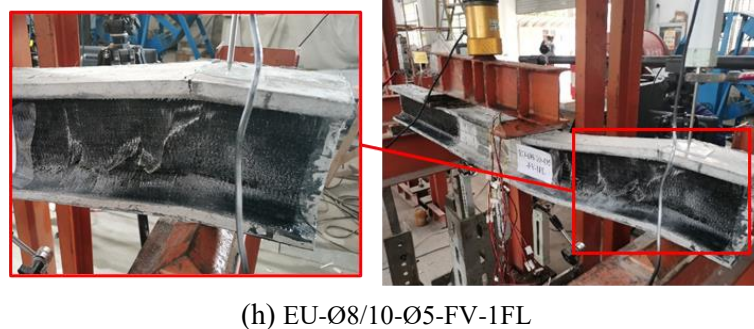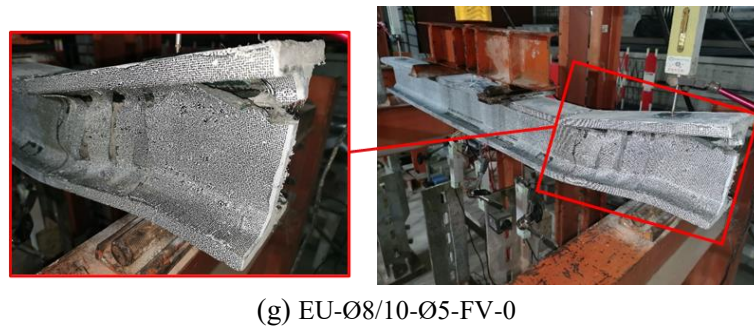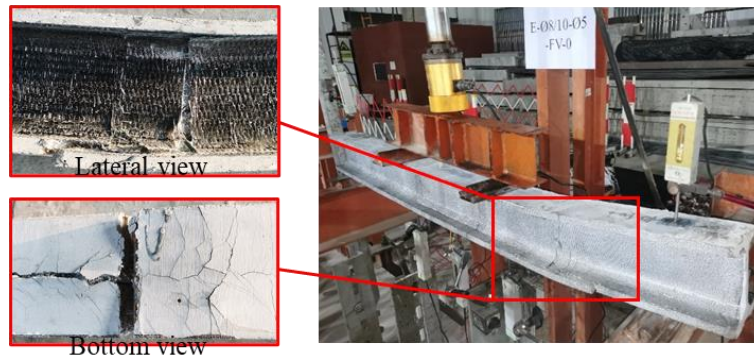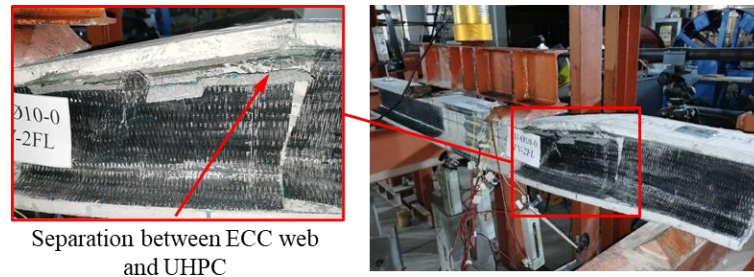
Fig. 5. Failure modes

Fig. 5f to Fig. 5i show the failure modes of specimens with two 8.0 mm HRB400 bars and one 10 mm HRB400 bar in the tensile flange, and 5.0 mm threaded rods at an interval of 50 mm in the web. As shown in Fig. 5f, when the E-Φ8/10-Φ5-FV-0 beam was damaged, the ECC bottom flange in

the bending shear zone was fractured at 100 mm away from the support. A long longitudinal crack that extended from the crack to the support was observed at the bottom of the beam. The analysis suggests that this is due to the thin protective layer and the expansion force caused by the tension of the steel bars at the beam end. As shown in Fig. 5g, when the EU-Φ8/10-Φ5-FV-0 beam was damaged, the top UHPC flange in the bending shear area was fractured at a distance of 150 mm away from the loading point, due to the presence of embedded vertical threaded rods, the UHPC flange and the ECC web did not separate as that in the EU-Φ10-0-FV-2FL beam. As shown in **Fig. 5**h, for the EU-Φ8/10-Φ5-FV-1F beam with one layer of BFRP sheet attached to the bottom of the beam, the UHPC flange in the bending shear area was fractured near the top of the support, and the ECC web was broken. The surface-attached BFRP sheets were peeled off from the ECC web due to shear cracks. As shown in **Fig. 5**i, when the BFRP at the bottom of the beam increased to two layers, the BFRP sheet that attached to the web of the EU-Φ8/10-Φ5-FV-2F beam was also debonded due to the generated oblique cracks. The upper flange UHPC and ECC web were dislocated, but also did not separate due to the presence of the embedded threaded rods.

Table 4. Summary of the cracks developing situation

Specimens No.	Cracks developing situation
E-0-0-0-0	A main crack appears in the mid-span, and dense micro-cracks appear on both sides of the main crack.
EU-0-0-0-0	The same to E-0-0-0-0
EU-Ø10-0-0-0	The dense and fine inclined cracks appeared in the bending-shear area
EU-Ø10-0-FV-1FL	the bottom flange and web in the flexural shear zone are dislocated along the beam length direction
EU-Ø10-0-FV-2FL	The top UHPC flange in the bending shear area is fractured upward from the loading point.
E-Ø8/10-Ø5-FV-0	The ECC bottom flange in the bending shear zone was fractured and a long longitudinal crack that extended from the crack to the support was observed at the bottom of the beam.
EU-Ø8/10-Ø5-FV-0	The top UHPC flange in the bending shear area was fractured.
EU-Ø8/10-Ø5-FV-1FL	The UHPC flange in the bending shear area was fractured near the top of the support and the ECC web was broken.
EU-Ø8/10-Ø5-FV-2FL	The BFRP sheet that attached to the web was debonded due to the generated oblique cracks.

4.2 Load vs. midspan displacement curves

Table 5. Summary of test results based on obtained curves

Specimens No.	Fcr (kN)	Fy (kN)	Fu (kN)	Δcr (mm)	Δy (mm)	Δu (mm)	Failure modes
E-0-0-0-0	2.1	-	3.5	0.87	-	11.45	ECC cracking
EU-0-0-0-0	2.6	-	3.2	1.07	-	5.19	ECC cracking
EU-Ø10-0-0-0	5.1	-	28.3	1.65	-	9.25	Shear failure
EU-Ø10-0-FV-1FL	5.3	-	29.2	0.72	-	9.57	Shear failure
EU-Ø10-0-FV-2FL	7.0	-	33.2	0.75	-	10.22	Shear failure
E-Ø8/10-Ø5-FV-0	3.6	22.8	26.5	0.62	4.94	16.36	Shear failure
EU-Ø8/10-Ø5-FV-0	5.5	-	38.0	0.62	-	5.27	Shear failure
EU-Ø8/10-Ø5-FV-1FL	4.9	-	41.8	0.58	-	6.09	Shear failure
EU-Ø8/10-Ø5-FV-2FL	4.8	-	43.3	0.42	-	5.77	Shear failure

Notes: Fcr, Fy, and Fu represent the cracking load, yielding load, and ultimate load, respectively; Δcr, Δy, and Δu represent the midspan displacement corresponding to the cracking load, yielding load, and ultimate load. The symbol "-" means not available.

Fig. 6 shows the load vs. midspan displacement (LD) curves of each test beam and the corresponding strain contours of the web along the beam length obtained by the 3D-digital image correlation (DIC) method under different load levels. The strain contours along the beam length can reflect the crack distribution mode of the beam to a certain extent. The characteristic loads, characteristic displacements, and failure modes of each test beam are summarized in **Table 4**. It

should be noted that, since most of the test beams are shear failures, except for the LD curve of the E-Ø8/10-Ø5-FV-0 beam, which shows an obvious yield segment, the other test beams have not yet entered the yielding stage, therefore, the f_y and Δ_y value of the other specimens in **Table 5** are not available except for the E-Ø8/10-Ø5-FV-0 beam. The influence of test parameters on the behavior of the composite beams is discussed in detail in the following section.
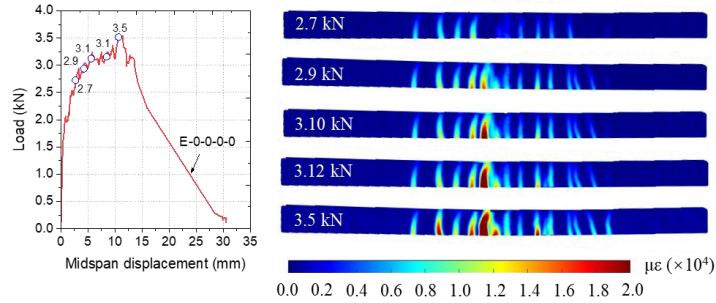
(a) E-0-0-0-0
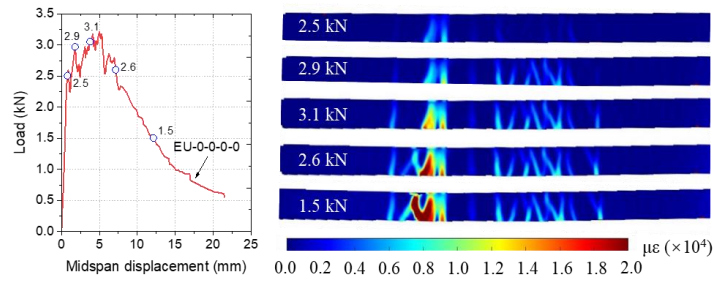
(b) EU-0-0-0-0
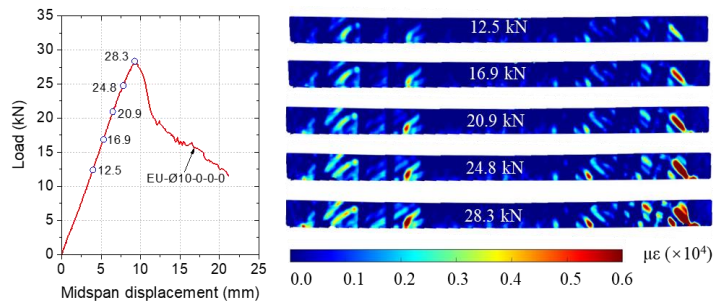
(c) EU-Ø10-0-0-0
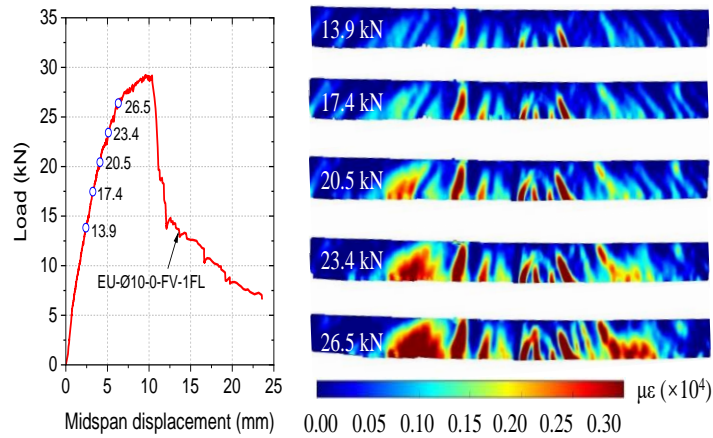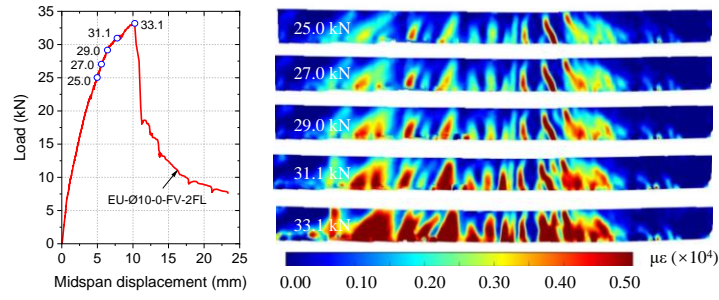
(d) EU-Ø10-0-FV-1FL

(e) EU-Ø10-0-FV-2FL
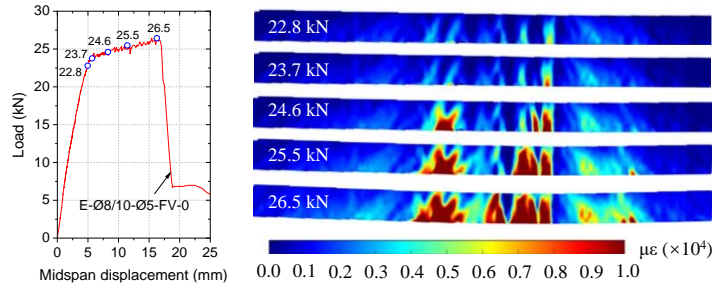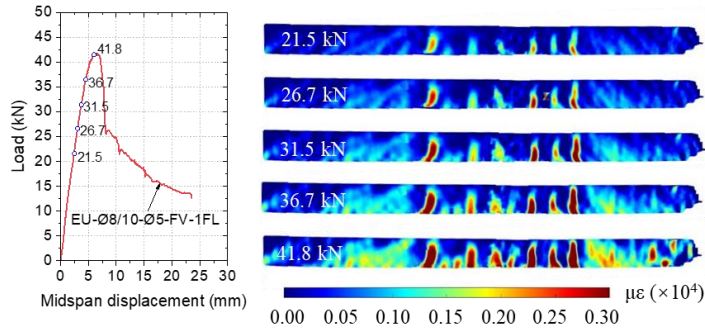
(f) E-Ø8/10-Ø5-FV-0
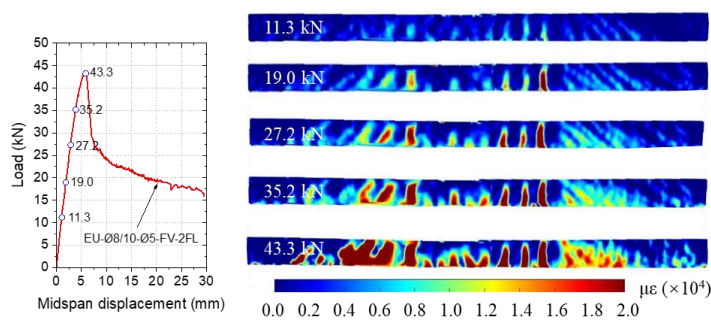
(g) EU-Ø8/10-Ø5-FV-0
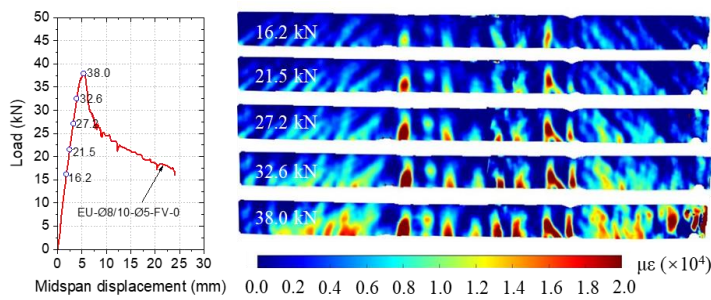
(h) EU-Ø8/10-Ø5-FV-1FL

(i) EU-Ø8/10-Ø5-FV-2FL
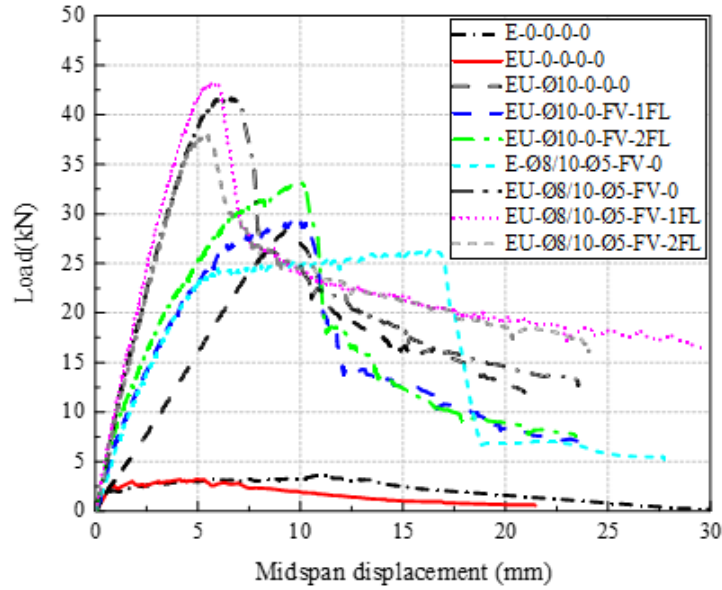
(j) Load-Midspan displacement curves

Fig. 6.   Load vs. midspan displacement curves

4.2.1 Effect of embedded tensile steel bars

The performance of I-shaped composite beams can be effectively improved by arranging steel reinforcement in the bottom ECC flange. Comparing **Fig. 6**b and Fig. 6c, it can be seen that after adding a 10 mm HRB400 steel bar to the bottom flange of the beam, the bearing capacity of the EU-Ø10-0-0-0 beam is significantly higher than that of the EU-0-0-0-0 beam. The failure mode is also changed from bending failure to shear failure. After configured with the inner steel bar, the ultimate load is increased from 3.2 kN to 28.3 kN, and the corresponding ultimate displacement is increased from 5.19 mm to 9.25 mm.

4.2.2 Effect of top UHPC flange

The top compression flange of the composite beam was UHPC. Comparing the E-0-0-0-0 beam and the EU-0-0-0-0 beam, it can be seen that for the un-reinforced beams, the replacement of UHPC in the top flange has little effect on the characteristic loads. The cracking load is slightly increased, while the ultimate load is slightly decreased. However, the flexural stiffness of the composite beam is significantly improved, for example, the ultimate displacement of the EU-0-0-0-0 beam is 54.7% lower than that of the E-0-0-0-0 beam. As the failure modes showed in **Fig. 6**a and **Fig. 6**b, the cracks of the pure ECC beam developed more finely and were more concentrated in the pure bending section. The main crack of the EU-0-0-0-0 beam was located at the loading point, and the cracks are relatively concentrated. In addition, as can be seen from the LD curves in **Fig. 6**a and **Fig. 6**b, both un-reinforced beams have good deformability due to the high tensile strain of ECC.

In the case of there is reinforcement in the bottom flange, as shown in **Fig. 6**f and **Fig. 6**g, compared with the pure E-Ø8/10-Ø5-FV-0 beam, the cracking load and ultimate load of the composite EU-Ø8/10-Ø5-FV-0 beam were both improved, especially the ultimate load, which has been increased by 30.3%. Due to the higher elastic modulus of UHPC, the flexural stiffness of the reinforced ECC/UHPC composite beam was significantly improved compared with the reinforced pure ECC beam, and the ultimate displacement of the EU-Ø8/10-Ø5-FV-0 beam was reduced by 67.8% compared with the E-Ø8/10-Ø5-FV-0 beam. Comparing the LD curves in **Fig. 6**f and **Fig. 6**g, it can be seen that the pure ECC beam had entered the flexural yielding stage, its flexural yielding load was 22.8 kN, and the corresponding mid-span displacement was 4.94 mm, while for the reinforced ECC/UHPC composite beam, it did not enter the flexural yielding stage, and the shear failure happened before the flexural failure.

4.2.3 Effect of bonded tensile BFRP sheet

Tensile BFRP sheets were attached to the bottom flange of part of the beams. As shown in **Fig. 6**g, **Fig. 6**h, and **Fig. 6**i, since the failure modes of the three beams, i.e., the EU-Ø8/10-Ø5-FV-0, EU-Ø8/10-Ø5-FV-1FL and EU-Ø8/10-Ø5-FV-2FL, were all shear failure, and the reinforcements in the web were all the same, there was no significant difference between the three test beams in terms of the LD curves. From the results in **Table 5**, it can be seen that the containing of the BFRP sheet on the cracking load is not significant, but the cracking displacement is reduced, and the ultimate load is slightly increased (maximum 12.2%). For the EU-Ø10-0-FV-1FL and the EU-Ø10-0-FV-2FL beams with a relatively lower reinforcement ratio in tension, the shear-resistance capacity has been improved by 12.0% when the BFRP layer increased from one to two, and the corresponding mid-span displacement was increased by 6.4%. Overall, in the case of a shear-dominated failure mode, the strength of the attached BFRP sheet at the bottom of the beam has not been fully exerted.

(a) E-0-0-0-0

(b) EU-0-0-0-0

(c) EU-Ø10-0-0-0

(d) EU-Ø10-0-FV-1FL

(e) EU-Ø10-0-FV-2FL

(f) E-Ø8/10-Ø5-FV-0

(g) EU-Ø8/10-Ø5-FV-0   (h) EU-Ø8/10-Ø5-FV-1FL
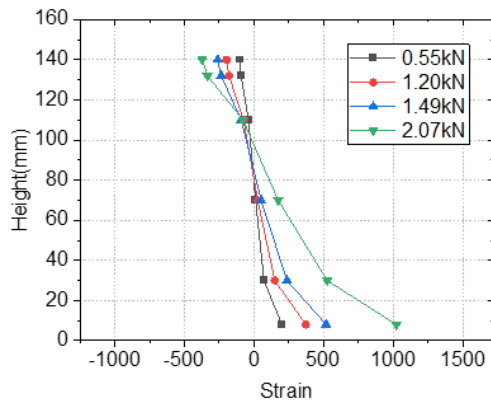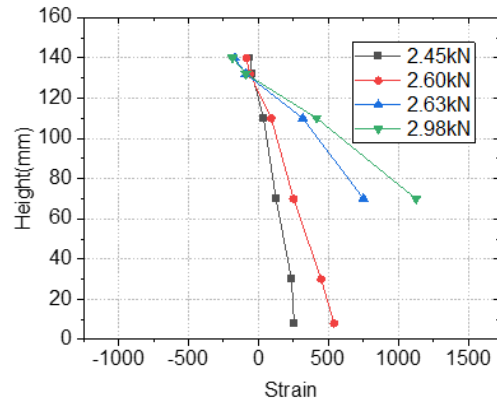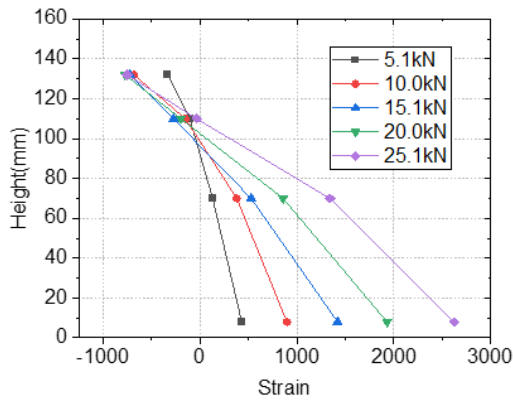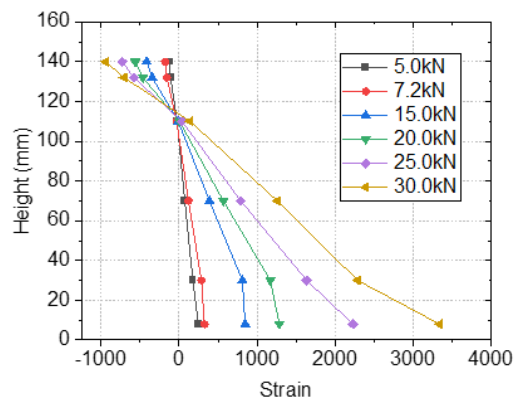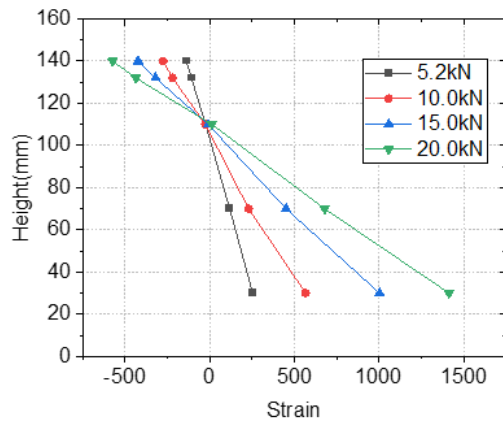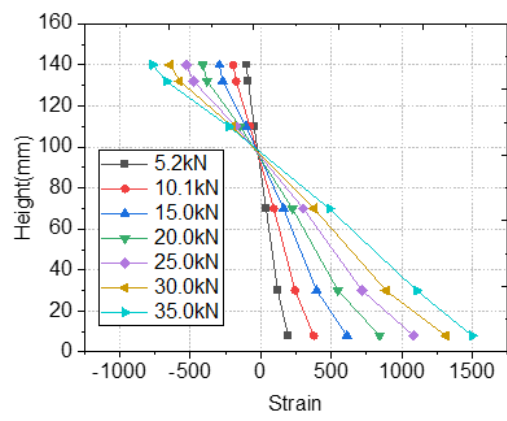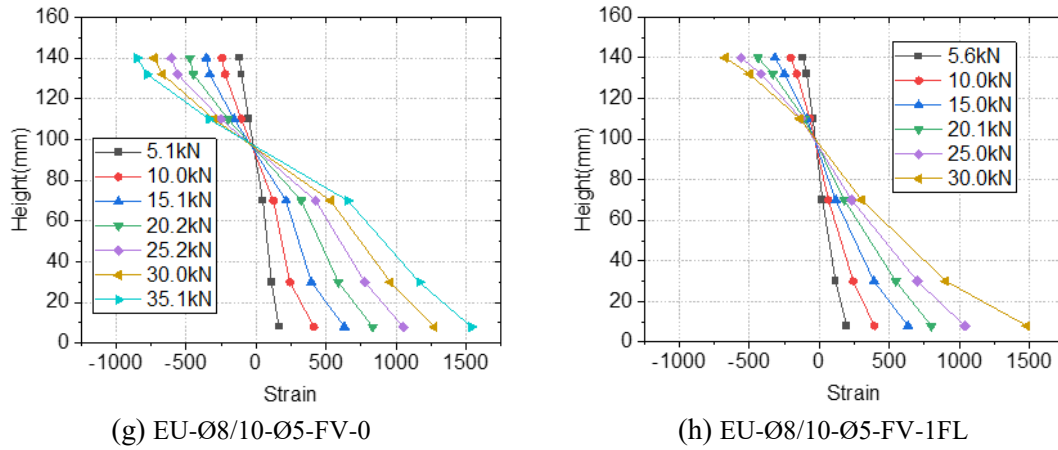
Fig. 7. Load vs. strain curves along the mid-span section of the I-shaped beams

4.3 Sectional strain distribution

Fig. 7 shows the variation of strain along the beam height with load at the mid-span of the tested beams. It can be seen that all beams in the pure bending section conform to the plane section assumption, which indicates that the casting process adopted in this paper can provide a satisfactory bond between the UHPC and ECC under flexural load. Comparing **Fig. 7**e and **Fig. 7**f, it can be seen that under the same load level, the tensile and compressive strains of the pure ECC beam (E-Ø8/10-Ø5-FV-0) are larger than those of the composite beam (EU-Ø8/10-Ø5-FV-0) at the same position, which also verifies the conclusion that the latter has a higher bending stiffness. In addition, comparing **Fig. 7**g and **Fig. 7**f, it can be seen that under the same load level, the tensile and compressive strains along the one-layer BFRP sheet attached beam height are larger than those of the beam with two layers of BFRP sheet at the same position, which also reflects the improvement effect of bonding BFRP sheet on the bending stiffness.

5 Conclusions

Based on the concept of the combined application of new materials, this paper innovatively proposed a new type of I-shaped ECC/UHPC composite beams, which are reinforced with internal reinforcements and external BFRP sheets in combination. The failure mode, load vs. mid-span displacement response, and bearing capacity under a four-point bending load were compared and analyzed. Based on this study, the following main conclusions are drawn:

(1) The top UHPC flange and the lower ECC web can cooperate well in the pure bending section. Setting steel bars in the bottom flange of the composite beam can greatly improve the performance. After configuring a 10 mm HRB400 steel bar, the ultimate load of the ECC/UHPC composite beam is increased from 3.2 kN to 28.3 kN, and the ultimate mid-span displacement is increased from 5.19 mm to 9.25 mm.

(2) Replacing the top flange of the I-shaped ECC beam with UHPC can improve the bending stiffness of the beam. In the case of no reinforcement, the ultimate mid-span displacement of the EU-0-0-0-0 beam is 54.7% lower than that of the E-0-0-0-0 beam. For the case of tensile reinforced with two 8.0 mm steel bars and one 10.0 mm steel bar, the replacement increased the ultimate load by 30.3% and the ultimate displacement by 67.8%.

(3) Since all the test beams suffered a shear failure, the effect of the bonded tensile BFRP sheet on improving the flexural strength was not fully exerted. However, it can be seen from the section strain data that the bending stiffness of the BFRP bonded beam was improved.

(4) The test confirmed that the shear bearing capacity of the ECC web in this paper is relatively low, and it is suggested that increasing the thickness of the web or using the UHPC web can be considered in subsequent studies.

Acknowledgments

Conflicts of interests

The authors declare that they have no known competing financial interests or personal relationships that could have appeared to influence the work reported in this paper.

Credit authorship contribution statement

Zhiqiang Dong: Conceptualization Investigation, Formal analysis, Writing – original draft, Funding acquisition. **Jianghao Ji**: Writing – original draft, Formal analysis. **Ziqing Liu**: Investigation, Formal analysis. **Chang Wu**: Supervision, Investigation, Validation. **Gang Wu**: Supervision, Funding acquisition. **Hong Zhu**: Supervision, Funding acquisition. **Pu Zhang**: Supervision, Validation.

References

[1] Fan JS, Guo SK, Ding R, Zhang J, Shi ZJ. Experimental and analytical research on the flexural behaviour of steel-ECC composite beams under negative bending moments. Engineering structure 2020; 210: 110309. https://doi.org/10.1016/j.engstruct.2020.110309.

[2] Cai JM, Pan JL, Tan JW, Vandevyvere B, Li XP. Behavior of ECC-encased CFST columns under eccentric loading. Journal of Building Engineering 2020; 30: 101188. https://doi.org/10.1016/j.jobe. 2020.101188.

[3] Cai JM, Pan JL, Li XP. Behavior of ECC-encased CFST columns under axial compression. Engineering structure 2018; 171: 1-9. https://doi.org/10.1016/j.engstruct.2018.05.090.

[4] Cai JM, Pan JL, Lu C. Mechanical behavior of ECC-encased CFST columns subjected to eccentric loading. Engineering structure 2018; 162: 22-28. https://doi.org/10.1016/j.engstruct.2018.02.029.

[5] Cai JM, Pan JL, Su H, Lu C. Experimental study on the hysteretic behavior of ECC-encased CFST columns. Engineering structure 2018; 173: 107-121. https://doi.org/10.1016/j.engstruct.2018.06.095.

[6] Zhang QT, Xiao JZ, Zhang KJ, Duan ZH. Mechanical behavior of seawater sea-sand recycled concrete columns confined by engineered cementitious composite under eccentric compression. Journal of Building Engineering 2021; 45:103497. https://doi.org/10.1016/j.jobe.2021.103497.

[7] Xiao JZ, Zhang QT, Yu JT, Ding T, Li Y, Shen J. A Novel Development of Concrete Structures: Composites Concrete Structures. Journal of Tongji University (Natural Science) 2018, 46(02): 147-155. https://doi.org/10.11908/j.issn.0253-374x.2018.02.001.

[8] Xiao JZ, Liu HR, Ding T, Ma GW. 3D printed concrete components and structures: an overview. Sustainable Structure Vol 1, No.2, 2021. https://doi.org/10.54113/j.sust.2021.000006.

[9] Perkowski Z, Czabak M, Grzeszczyk S, Fraczek D, Tatara K, Matuszek-Chmurowska A, Jurowski K, Jedraszak B. Experimental Research on Concrete Beams Reinforced with High Ductility Steel Bars and Strengthened with a Reactive Powder Concrete Layer in the Compression Zone. Materials 2020; 13(18): 4173. https://doi.org/10.3390/ma13184173.

[10] Wang Z, Nie X, Fan JS, Lu XY, Ding R. Experimental and numerical investigation of the interfacial properties of non-steam-cured UHPC-steel composite beams. Construction and Building Materials 2019; 195: 323-339. https://doi.org/10.1016/j.conbuildmat.2018.11.05.

[11] Zhang Y, Cai SK, Zhu YP, Fan L, Shao XD. Flexural responses of steel-UHPC composite beams under hogging moment. Engineering structure 2020; 206: 110134. https://doi.org/10.1016/j.engstruct. 2019. 110134.

[12] Wang JQ, Qi JA, Tong T, Xu QZ, Xiu HL. Static behavior of large stud shear connectors in steel-UHPC composite structures. Engineering structure 2019; 178: 534-542. https://doi.org/10.1016/j.engstruct. 2018. 07.058.

[13] Yoo SW, Choi YC, Choi JH, Choo JF. Nonlinear flexural analysis of composite beam with Inverted-T steel girder and UHPC slab considering partial interaction. Journal of Building Engineering 2021; 34: 101887. https://doi.org/10.1016/j.jobe.2020.101887.

[14] Yoo SW, Choo JF. Evaluation of the flexural behavior of composite beam with inverted-T steel girder and steel fiber reinforced ultra-high performance concrete slab. Engineering structure 2016; 118: 1-15. https://doi.org/10.1016/j.engstruct.2016.03.052.

[15] Davids WG, Diba A, Dagher HJ, Guzzi D, Schanck AP. Development, assessment and implementation of a

novel FRP composite girder bridge. Construction and Building Materials 2022; 340: 127818. https://doi.org/10.1016/j.conbuildmat.2022.127818.

[16] Feng P, Li ZY, Wang J, Liu TQ. Novel joint for pultruded FRP beams and concrete-filled FRP columns: Conceptual and experimental investigations. Composite Structures 2022; 287: 115339. https://doi.org/10.1016/j.compstruct.2022.115339.

[17] Huang ZJ, Chen WS, Tran TT, Pham TM, Hao H, Chen ZY, Elchalakani M. Experimental and numerical study on concrete beams reinforced with Basalt FRP bars under static and impact loads. Composite Structures 2021; 263: 113648. https://doi.org/10.1016/j.compstruct.2021.113648.

[18] Peng F, Xue WC. Experimental investigation on shear behavior of FRP post-tensioned concrete beams without stirrups. Engineering structure 2021; 244: 112835. https://doi.org/ 10.1016/j.engstruct.2021.112835.

[19] Ali AH, Mohamed HM, Chalioris CE, Deifalla A. Evaluating the shear design equations of FRP-reinforced concrete beams without shear reinforcement. Engineering structure 2021; 235: 112017. https://doi.org/10.1016/j.engstruct.2021.112017.

[20] Zhou YW, Sui LL, Huang XX, Guo MH, Luo MS, Hu B, Chen C. Enhancing the EB-FRP strengthening effectiveness by incorporating a cracking-control layer of ECC with different thicknesses. Construction and Building Materials 2021; 286: 122975. https://doi.org/10.1016/j.conbuildmat.2021.122975.

[21] Hu B, Zhou YW, Xing F, Sui LL, Luo MS. Experimental and theoretical investigation on the hybrid CFRP-ECC flexural strengthening of RC beams with corroded longitudinal reinforcement. Engineering structure 2019; 200: 109717. https://doi.org/ 10.1016/j.engstruct.2019.109717.

[22] Wu C, Li VC. CFRP-ECC hybrid for strengthening of the concrete structures. Composite Structures 2017; 178: 372-382. https://doi.org/ 10.1016/j.compstruct.2017.07.034.

[23] Yang X, Gao WY, Dai JG, Lu ZD, Yu KQ. Flexural strengthening of RC beams with CFRP grid-reinforced ECC matrix. Composite Structures 2018; 189: 9-26. https://doi.org/10.1016/j. compstruct.2018.01.048.

[24] Zheng AH, Liu ZZ, Li FP, Li S. Experimental investigation of corrosion-damaged RC beams strengthened in flexure with FRP grid-reinforced ECC matrix composites. Engineering structure 2021. 244: 112779. https://doi.org/10.1016/j.engstruct.2021.112779.

[25] Zheng YZ, Wang WW, Mosalam KM, Fang Q, Chen L, Zhu ZF. Experimental investigation and numerical analysis of RC beams shear strengthened with FRP/ECC composite layer. Composite Structures 2020; 246: 112436. https://doi.org/10.1016/j.compstruct.2020.112436.

[26] Guo R, Ren Y, Li MQ, Hu P, Du M, Zhang R. Experimental study on flexural shear strengthening effect on low-strength RC beams by using FRP grid and ECC. Engineering structure 2021; 227: 111434. https://doi.org/10.1016/j.engstruct.2020.111434.

[27] Wang LC, Yin SP, Hua YT. Flexural behavior of BFRP reinforced seawater sea-sand concrete beams with textile reinforced ECC tension zone cover. Construction and Building Materials 2021; 278: 122372. https://doi.org/10.1016/j.conbuildmat.2021.122372.

[28] Ge WJ, Ashour AF, Cao DF, Lu WG, Gao PQ, Yu JM, Ji X, Cai C. Experimental study on flexural behavior of ECC-concrete composite beams reinforced with FRP bars. Composite Structures 2019; 208: 454-465. https://doi.org/ 10.1016/j.compstruct.2018.10.026.

[29] Ge WJ, Tang R, Wang Y, Zhang ZW, Sun CZ, Yao S, Lu WG. et al., Flexural performance of ECC-concrete composite beams strengthened with carbon fiber sheet. Result In Engineering 2022; 13: 100334. https://doi.org/10.1016/j.rineng.2022.100334.

[30] Ge WJ, Song WR, Ashour AF, Lu WG, Cao DF. Flexural performance of FRP/steel hybrid reinforced engineered cementitious composite beams. Journal of Building Engineering 2020; 31: 101329. https://doi.org/10.1016/j.jobe.2020.101329.

[31] Yuan F, Chen MC, Pan JL. M. Experimental study on seismic behaviours of hybrid FRP–steel-reinforced ECC–concrete composite columns. Composites Part B-Engineering 2019; 176: 107272. https://doi.org/10.1016/j.compositesb.2019.107272.

[32] Moon J, Taha MMR, Kim JJ. Flexural strengthening of RC slabs using a hybrid FRP-UHPC system including shear connector. Advances in Materials Science and Engineering. 2017; 4387545. https://doi.org/ 10.1155/2017/4387545.

[33] Elsanadedy HM, Abbas H, Almusallam TH, Al-Salloum YA. Hybrid UHPC/NSM CFRP strips vs. traditional systems for flexural upgrading of RC beams–Experimental and FE study. Composite Structures 2021; 261: 113291. https://doi.org/10.1016/j.compstruct.2020.113291.

[34] Chen C, Cai HY, Cheng LJ. Shear strengthening of corroded RC beams using UHPC–FRP composites. Journal of Building Engineering 2021; 26(1): 04020111. https://doi.org/10.1061/(ASCE)BE.1943-5592.0001653.

[35] Ferrier E, Confrere A, Michel L, Chanvillard G, Bernardi S. Shear behaviour of new beams made of UHPC concrete and FRP rebar. Composites Part B-Engineering 2016; 90: 1-13. https://doi.org/10.1016/j.compositesb.2015.11.022.

[36] Zagon R, Matthys S, Kiss Z. Shear behaviour of SFR-UHPC I-shaped beams. Construction and Building Materials 2016; 124: 258-268. https://doi.org/10.1016/j.conbuildmat.2016.07.075.

[37] Ferrier E, Michel L, Zuber B, Chanvillard G. Mechanical behaviour of ultra-high-performance short-fibre-reinforced concrete beams with internal fibre reinforced polymer bars. Composites Part B-Engineering 2015; 68: 246-258. https://doi.org/10.1016/j.compositesb.2014.08.001.

[38] Randl N, Mészöly T, Harsányi P. Shear behaviour of UHPC beams with varying degrees of fibre and shear reinforcement, in High Tech Concrete: Where Technology and Engineering Meet. 2018; Springer. 500-507. https://doi.org/10.1007/978-3-319-59471-2_60.

[39] Xu XQ, Hou ZJ. Experimental Study on One-Way BFRP Bar-Reinforced UHPC Slabs under Concentrated Load. Materials 2020; 13(14): 3077. https://doi.org/10.3390/ma13143077.

[40] Meng WN, Khayat KH, Bao Y. Flexural behaviors of fiber-reinforced polymer fabric reinforced ultra-high-performance concrete panels. Cement and Concrete Composites. 2018; 93: 43-53. https://doi.org/110.1016/j.cemconcomp.2018.06.012.

[41] Ye YY, Smith ST, Zeng JJ, Zhuge Y, Quach WM. Novel ultra-high-performance concrete composite plates reinforced with FRP grid: Development and mechanical behaviour. Composite Structures 2021; 269: 114033. https://doi.org/10.1016/j.compstruct.2021.114033.

[42] Al-Ramahee MA, Chan T, Mackie KR, Ghasemi S, Mirmiran A. Lightweight UHPC-FRP composite deck system. Journal of Building Engineering 2017; 22(7): 04017022. https://doi.org/10.1061/(ASCE)BE.194 3-5592.0001049.

[43] Dong ZQ, Wu G, Zhao XL, Zhu H, Shao XX. Behaviors of hybrid beams composed of seawater sea-sand concrete (SWSSC) and a prefabricated UHPC shell reinforced with FRP bars. Construction and Building Materials 2019; 213: 32-42. https://doi.org/10.1016/j.conbuildmat.2019.04.059.

[44] Dong ZQ, Wu G, Zhu H, Zhao XL, Wei Y, Qian H. Flexural behavior of seawater sea-sand coral concrete–UHPC composite beams reinforced with BFRP bars. Construction and Building Materials 2020; 265: 120279. https://doi.org/10.1016/j.conbuildmat.2020.120279.

[45] El-Hacha R, Chen D. Behaviour of hybrid FRP–UHPC beams subjected to static flexural loading. Composites Part B-Engineering 2012; 43(2): 582-593. https://doi.org/10.1016/j.compositesb.2011.07.004.

[46] Chen D, El-Hacha R. Behaviour of hybrid FRP–UHPC beams in flexure under fatigue loading. Composite Structures 2011; 94(1): 253-266. https://doi.org/10.1016/j.compstruct.2011.06.016.

[47] Chen D, El-Hacha R. Damage tolerance and residual strength of hybrid FRP–UHPC beam. Engineering structure 2013; 49: 275-283. https://doi.org/10.1016/j.engstruct.2012.11.016.

[48] Iskander M, El-Hacha R, Shrive N. Governing failure criterion of short-span hybrid FRP-UHPC beams subjected to high shear forces. Composite Structures 2018; 185: 123-131. https://doi.org/10.1016/j.compstruct. 2017.11.003.

[49] Zou XX, Feng P, Wang JQ. Bolted shear connection of FRP-concrete hybrid beams. Journal of Composites for construction. 2018; 22(3): 04018012. https://doi.org/10.1061/(ASCE)CC. 1943-5614.000 0845.

[50] Zou XX, Wang JQ. Experimental study on joints and flexural behavior of FRP truss-UHPC hybrid bridge. Composite Structures 2018; 203: 414-424. https://doi.org/10.1016/j.compstruct.2018.06.118.

[51] Zhang P, Hu R, Zhou XX, Liu Y, Li QL, Wu G, Sheikh SA. Experimental study of a novel continuous FRP-UHPC Hybrid Beam. Composite Structures 2021; 261: 113329. https://doi.org/10.1016/j. compstruct. 2020.113329.

[52] Zhang P, Lv XL, Liu Y, Zou XX, Li YZ, Wang JQ, Sheikh SA. Novel fiber reinforced polymers (FRP)-ultrahigh performance concrete (UHPC) hybrid beams with improved shear performance. Construction and Building Materials 2021; 286: 122720. https://doi.org/10.1016/j.conbuildmat. 2021.1227 20.

[53] Zohrevand P, Mirmiran A. Stress-strain model of ultrahigh performance concrete confined by fiber-reinforced polymers. Journal of Materials in Civil Engineering. 2013; 25(12): 1822-1829. https:// doi.org/10.1061/(ASCE)MT.1943-5533.0000769.

[54] Zohrevand P, Mirmiran A. Behavior of ultrahigh-performance concrete confined by fiber-reinforced polymers. Journal of Materials in Civil Engineering 2011; 23(12): 1727-1734. https://doi.org/10.1061/ (ASCE) MT.1943-5533.0000324.

[55] Wang WQ, Wu CQ, Liu ZX, Si HL. Compressive behavior of ultra-high performance fiber-reinforced concrete (UHPFRC) confined with FRP. Composite Structures 2018; 204: 419-437. https://doi.org/10.101 6/ j.compstruct.2018.07.102.

[56] Tian HW, Zhou Z, Wei Y, Wang YQ. Behavior of FRP-confined ultra-high performance concrete under eccentric compression. Composite Structures 2021; 256: 113040. https://doi.org/10.1016/j.compstruct.202 0.113040.

[57] Tian HW, Zhou Z, Wei Y, Wang YQ, Lu JP. Experimental investigation on axial compressive behavior of ultra-high performance concrete (UHPC) filled glass FRP tubes. Construction and Building Materials 2019; 225: 678-691. https://doi.org/10.1016/j.conbuildmat.2019.07.204.

[58] Tian HW, Zhou Z, Wei Y, Lu JP. Behavior and Modeling of Ultra-High Performance Concrete-Filled FRP Tubes under Cyclic Axial Compression. Journal of Composites for construction 2020; 24(5): 04020045. https://doi.org/10.1061/(ASCE)CC.1943-5614.0001060.

[59] Guler S. Axial behavior of FRP-wrapped circular ultra-high performance concrete specimens. Structural Engineering and Mechanics. 2014; 50(6): 709-722. https://doi.org/10.12989/sem.2014.50.6.709.

[60] Deng ZC, Qu JL. The experimental studies on behavior of ultrahigh-performance concrete confined by hybrid fiber-reinforced polymer tubes. Advances in Materials Science and Engineering 2015; 201289. https://doi.org/10.1155/2015/201289.

[61] Liao JJ, Zeng JJ, Gong QM, Quach WM, Gao WY, Zhang LH. Design-oriented stress-strain model for FRP-confined ultra-high performance concrete (UHPC). Construction and Building Materials 2022; 318: 126200. https://doi.org/10.1016/j.conbuildmat.2021.126200.

[62] Zeng JJ, Long TW. Compressive Behavior of FRP Grid-Reinforced UHPC Tubular Columns. Polymers 2021; 14(1): 125. https://doi.org/10.3390/polym14010125.

[63] Zeng JJ, Chen SP, Peng KD, Dai JG. Novel FRP micro-bar reinforced UHPC permanent formwork for circular columns: Concept and compressive behavior. Composite Structures 2022; 285: 115268. https://doi.org/10.1016/j.compstruct.2022.115268.